



 Cite this: *RSC Adv.*, 2024, 14, 17296

Fabrication and characterization of inorganic–organic hybrid copper ferrite anchored on chitosan Schiff base as a reusable green catalyst for the synthesis of indeno[1,2-*b*]indolone derivatives†

 Hannaneh Hassanpour and Hossein Naeimi *

This study presents a description of the catalytic synthesis of indeno[1,2-*b*]indolone derivatives. In this method, initially, a Schiff base compound was synthesized from the reaction of acetylacetone with 2-hydroxyaniline. Then, the prepared Schiff base was immobilized on chelated magnetic copper ferrite nanoparticles with a chitosan surface to design and prepare the CuFe₂O₄@CS-SB nanocomposite. Further, the one-pot multi-component cyclization reaction of aniline, dimedone and ninhydrin was conducted using the synthesized nanocomposite as a heterogeneous acid catalyst in water solvent under thermal conditions. In this reaction, the products were obtained in excellent yields and short reaction times, and the catalyst could be recycled and reused six times without any loss in product yields. By conducting FT-IR spectroscopy, ¹H NMR spectroscopy, XRD, FE-SEM, TGA, elemental mapping scanning, EDX and BET analyses, the structure of the nanocatalyst was characterized. In addition, for the identification of organic compounds, FT-IR, ¹H NMR, and ¹³C NMR spectroscopies and melting point analysis were used, which confirmed the synthesis of this class of derivatives.

 Received 20th December 2023
 Accepted 29th April 2024

DOI: 10.1039/d3ra08705k

rsc.li/rsc-advances

1. Introduction

Indeno[1,2-*b*]indolones are a significant class of heterocyclic organic compounds that are used in biology and pharmacology.^{1,2} The most known simple heterocyclic compounds are pyridine, pyrrole, furan and thiophene.³ Heterocyclic compounds make up about sixty-five percent of organic chemistry, and they play a vital role in the metabolism of all living cells. A large number of heterocyclic compounds, both synthetic and natural, are pharmacologically active.⁴ Due to their ability to suppress lipid peroxidation, this class of pharmaceuticals has attracted a substantial amount of attention.^{5,6} Protein kinase inhibitors, in addition to being adenosine triphosphate/guanosine triphosphate-competitive inhibitors, are potassium channel openers and estrogenic drugs.⁷ Indeno[1,2-*b*]indolones occupy a special role in a few more non-cancer (diseases associated with angiogenesis, viral infections, inflammatory markers, and neurodegenerative disorders) and cancer ailments (such as prostate, colon, breast and lung cancers).⁸ In 2016, Liu and colleagues used lactic acid as a homogeneous catalyst to synthesize indeno[1,2-*b*]indolone compounds. The working method is abrasive and solvent-free, and it is done within 10

minutes at room temperature.⁹ In 2018, Safari and his co-worker used MMT@Fe₃O₄ as a heterogeneous catalyst and prepared derivatives of indeno[1,2-*b*]indolones in water as a solvent at 70 °C.² In chemical reactions, the use of heterogeneous catalysts is very significant because of their solid form, which is in contrast to the homogeneous catalyst phase.^{10,11}

Recently, a heterogeneous catalyst has been formed with purposeful design and preparation, which has active sites on its surface to enable it to bond to organic compounds to promote the reaction.¹²

Chitosan is a derivative of chitin and is a polysaccharide.¹³ It is a type of heteropolymer that is formed from the deacetylation of chitin and acetyl glucosamine groups though its deacetylation is incomplete.¹⁴ Stable activities of chitosan in the field of catalysis with magnetic separation capability and a copper ferrite nanocomposite made of chitosan have been reported.¹⁵ Chitosan is a substance that is environmentally friendly, and because of the increasing attention toward green chemistry, the use of this substance becomes important.¹⁶ Recently, it has been reported that chitosan may be used to inhibit fibroplasia in wound healing and promote tissue growth and differentiation.¹⁷ Chitosan can act as a catalytic substrate in many reactions, and it also dissolves in dilute acetic acid and activates its surface.¹⁸ The existence of interactions between metal and OH groups on the surface of chitosan has recently attracted increasing attention for the fabrication of complex materials.¹⁹ It is due to the presence of NH₂ on the surface of chitosan that it allows

Department of Organic Chemistry, Faculty of Chemistry, University of Kashan, Kashan, 87317-51167, I.R. Iran. E-mail: naeimi@kashanu.ac.ir; Fax: +983155912397; Tel: +983155912388

† Electronic supplementary information (ESI) available. See DOI: <https://doi.org/10.1039/d3ra08705k>



copolymerization using monomers to achieve unique properties.²⁰ Also, the reason for using magnetic nanoparticles in the synthesis of the catalyst can be attributed to their two general characteristics: effects that are limited to the size of their particles and effects that are superficial and cause special characteristics in magnetic nanoparticles.²¹

Schiff bases can act as ligands and bind on the chitosan substrate.²² A Schiff base can be formed by the reaction between an aldehyde or a ketone with a primary amine under various conditions.²³ Organic compounds used as Schiff bases have attracted the attention of many scientists in various fields, including industry and pharmaceuticals.²⁴ Also, these compounds have biological activities.²⁵

In continuation of our ongoing research works on catalytic reactions,^{26–31} in this work, we chose to look into the straightforward and efficient synthesis of indeno[1,2-*b*]indolones utilizing a novel effective heterogeneous nanocatalyst. Initially, copper ferrite nanoparticles were prepared by the coprecipitation method; then, the magnetic nanoparticles of the CuFe₂O₄@CS-SB nanocomposite were prepared by chelating on the surface of chitosan and a Schiff base. This prepared nanocomposite had the ability to catalyze the one-pot, three-component reaction between ninhydrin, dimedone and aniline derivatives as a nano-solid acid.

2. Experimental section

2.1. Substances and apparatus

The chemicals and solvents used were of high quality from Merck, Fluka and Aldrich Chemical Companies without the need for further purification. FT-IR spectra were recorded using a PerkinElmer 550 spectrometer with KBr pellets in the range of 400–4000 cm⁻¹ to observe the functional groups. Proton and carbon nuclear magnetic resonance spectroscopy was done with the internal reference in DMSO-d₆ solvent to determine the structure of the products. The melting point is one of the important physical parameters that is checked for the purity of a given sample and compared with the existing literature, which was done using an Electrothermal Mk3 instrument in this study. The fabricated catalyst was characterized using ATR, XRD, FE-SEM, EDX, VSM, BET and TGA techniques. ATR technique uses the property of internal reflection in the sample along with infrared spectroscopy, where samples are provided in solid or liquid state without preparation. In this study, an iCE 3500 spectrometer made by Thermo Scientific Company was employed. Powder X-ray diffraction (XRD) is a rapid analytical technique for the characterization of the nanostructure, which was utilizing Cu wavelength (1.54 Å). FE-SEM analysis examined minor area contamination spots at 15 kV electron accelerating voltages with well-matched EDS results obtained from a ZEISS SIGMAVP apparatus. VSM was used as a specific device for the determination of the magnetic properties of the nanocatalyst by a PPMS-9 T device at 300 K. BET analysis was done to measure the specific surface area of the materials. TGA was carried out for the samples under controlled temperature conditions in an air atmosphere with a 10 °C min⁻¹ heating rate *via* a METTLER-810 analyzer.

2.2. Procedure for synthesis of 4-(2-hydroxyaniline)pent-3-en-2-one

Schiff base was formed with an ethanolic solution of 5 mmol acetylacetone and an ethanolic solution of 5 mmol 2-aminophenol. The ethanolic solution obtained from the amine was added dropwise to the ketone ethanolic solution. Thereafter, the reaction mixture was refluxed at 80 °C for 6 h; after that, the reaction was checked by TLC until completion, following which yellow crystals were formed. They were washed with ethanol and diethylether, and the resulting product was obtained with a yield of 97%. ATR (cm⁻¹): 3010, 2721, 2599, 1585, 1552, 1501, 1434, 1308, 1102, 745; ¹H NMR (400 MHz, DMSO-d₆) (ppm): 12.15 (s, 1H, NH), 9.91 (s, 1H, OH), 7.16 (d, *J* = 8.0 Hz, 1H), 7.02 (t, *J* = 4.0 Hz, 1H), 6.91 (d, *J* = 4.0 Hz, 1H), 6.79 (t, *J* = 8.0 Hz, 1H), 5.20 (s, 1H), 1.97 (s, 6H, 2 CH₃).

2.3. Synthetic process of chitosan-Schiff base (CS-SB)

After dissolving 1.000 g of 4-(2-hydroxyaniline)pent-3-en-2-one in methanolic solution, 1.000 g of weighed chitosan was dissolved in methanol and glacial acetic acid (95 : 5 v/v). After 2 hours, the Schiff base solution was added drop by drop to the chitosan suspension. The reaction mixture was then refluxed for 24 h at 80 °C. After making sure that the reaction was completed, the reaction mixture was centrifuged (5000 rpm for 5 min) and washed several times with methanol and acetone. Soxhlet extraction (using methanol and acetone solvents for 24 h) was used to extract the interfering metals from chitosan. Then, the obtained product was dried in an oven at 60 °C for 24 h, yielding a brown powder that indicated the final synthetic product.

2.4. A procedure for the synthesis of magnetic CuFe₂O₄ NPs

5.406 g (20 mmol) of FeCl₃·6H₂O and 1.704 g (10 mmol) of CuCl₂·2H₂O were mixed together, then subjected to ultrasonic waves for 15 minutes, then stirred for 15 min at room temperature. Next, 3 M NaOH solution was added drop by drop to the obtained mixture until the pH was 13 and a precipitate was obtained. After reaching the desired pH, 3 drops of oleic acid were added to the reaction mixture as a surfactant and refluxed at 80 °C for 50 min. After cooling the reaction mixture, it was centrifuged (5000 rpm for 5 min), washed with deionized water and ethanol several times, and dried in an oven at 80 °C. In order to calcine the product, it was placed in a furnace at 800 °C for 10 h, and the CuFe₂O₄ NPs (nanoparticles) were formed.

2.5. General procedure for the synthesis of the CuFe₂O₄@CS-SB catalyst

0.500 g of CuFe₂O₄ NPs in 100 mL of deionized water was subjected to ultrasonic waves to disperse the nanoparticles in the solvent. 0.500 g of Schiff base-chitosan was added to the previous solution, and the suspension was stirred for 1 h at 50 °C. Then, 0.2 M NaOH solution was added drop by drop to the suspension to form a black precipitate. In the last step, 25% ammonia was added to the solution and the reaction was stirred for 30 minutes at the desired temperature. The product was

centrifuged (5000 rpm for 5 min), washed several times with deionized water to neutralize, dried in an oven at 70 °C for 12 h, and stored in a desiccator for future usage (Fig. S1 in the ESI†).

2.6. General procedure for the synthesis of indeno[1,2-*b*]indolone

Exact amounts of aromatic amine (1 mmol), 1 mmol of dime-done and CuFe₂O₄@CS-SB catalyst (0.004 g) were stirred in distilled water at 75 °C. Subsequently, 1 mmol of ninhydrin was added and the reaction mixture was stirred again for a suitable time. The reaction progress was checked by thin layer chromatography (TLC), and the reaction mixture was filtered off after completion. With the aim of achieving the CuFe₂O₄@CS-SB catalyst from the products, the CuFe₂O₄@CS-SB catalyst was separated from the reaction mixture by a strong external magnet and washed several times with acetone and ethanol to be used as a catalyst in other reactions. Ultimately, the precipitate was washed by petroleum ether and recrystallized from ethanol, if required, to give the absolute target products. Every single product was confirmed by determining its melting point and applying spectroscopic methods such as FT-IR, ¹H NMR and ¹³C NMR.

2.7. Spectroscopic and physical data for the synthesized indeno[1,2-*b*]indolone derivatives

2.7.1. 4*b*,9*b*-Dihydroxy-7,7-dimethyl-5-phenyl-4*b*,5,6,7,8,9*b*-hexahydroindeno[1,2-*b*]indole-9,10-dione (4a). White solid (93% yield); m.p._{rep.} = 260–265 °C (ethanol); m.p._{lit.} = 255–257 °C;² IR (KBr) ν (cm⁻¹): 3475, 3232, 2931, 2876, 1723, 1606, 1547, 1452, 1277, 1159; ¹H NMR (400 MHz, DMSO-*d*₆) δ (ppm) = 7.72 (d, *J* = 4.0 Hz, 1H, ArH), 7.58–7.45 (m, 5H, ArH), 7.30 (s, 2H, ArH), 7.28 (s, 1H), 6.60 (d, *J* = 8.0 Hz, 1H, ArH), 6.01 (s, 1H), 2.41 (d, *J* = 16.0 Hz, 1H), 2.15 (d, *J* = 16.0 Hz, 1H), 1.91 (d, *J* = 16.0 Hz, 1H), 1.79 (d, *J* = 16.0 Hz, 1H), 0.96 (s, 3H, Me), 0.89 (s, 3H, Me).

2.7.2. 5-(4-Ethylphenyl)-4*b*,9*b*-dihydroxy-7,7-dimethyl-4*b*,5,6,7,8,9*b*-hexahydroindeno[1,2-*b*]indole-9,10-dione (4b). Light brown solid (92% yield); m.p._{rep.} = 145–150 °C (ethanol); IR (KBr) ν (cm⁻¹): 3398, 2956, 2876, 1724, 1610, 1551, 1156; ¹H NMR (400 MHz, DMSO-*d*₆) δ (ppm) = 7.72 (d, *J* = 4.0 Hz, 1H, ArH), 7.59–7.51 (m, 2H, ArH), 7.33 (d, *J* = 8.0 Hz, 3H, ArH), 7.21 (s, 2H, ArH), 7.19 (s, 1H), 6.66 (d, *J* = 8.0 Hz, 1H, ArH), 5.97 (s, 1H), 2.7 (d, *J* = 8.0 Hz, 2H, CH₂), 2.37 (d, *J* = 16.0 Hz, 1H), 2.13 (d, *J* = 16.0 Hz, 1H), 1.90 (d, *J* = 16.0 Hz, 1H), 1.79 (d, *J* = 16.0 Hz, 1H), 1.25 (t, *J* = 8.0 Hz, 3H, Me), 0.88 (s, 3H, Me), 0.86 (s, 3H, Me); ¹³C NMR (100 MHz, DMSO-*d*₆) δ (ppm) = 198.07, 189.57, 147.73, 144.01, 135.30, 135.20, 133.97, 130.62, 129.76, 128.72, 125.41, 123.62, 105.68, 97.10, 83.87, 51.66, 37.47, 33.87, 29.78, 28.27, 27.03, 15.85.

2.7.3. 5-(3-Chlorophenyl)-4*b*,9*b*-dihydroxy-7,7-dimethyl-4*b*,5,6,7,8,9*b*-hexahydroindeno[1,2-*b*]indole-9,10-dione (4c). White solid (90% yield); m.p._{rep.} = 220–225 °C (ethanol); m.p._{lit.} = 223–226 °C;³² IR (KBr) ν (cm⁻¹): 3564, 3391, 2947, 2873, 1719, 1641, 1480, 1159, 731; ¹H NMR (400 MHz, DMSO-*d*₆) δ (ppm) = 7.61 (d, *J* = 4.0 Hz, 1H, ArH), 7.51–7.56 (m, 5H, ArH), 7.30 (s, 1H, ArH), 7.18 (d, *J* = 8.0, 1H, ArH), 2.48 (d, *J* = 16.0 Hz, 1H), 2.15 (d,

J = 16.0 Hz, 1H), 1.90 (d, *J* = 16.0 Hz, 1H), 1.81 (d, *J* = 16.0 Hz, 1H), 0.96 (s, 3H, Me), 0.91 (s, 3H, Me).

2.7.4. 5-(4-Bromophenyl)-4*b*,9*b*-dihydroxy-7,7-dimethyl-4*b*,5,6,7,8,9*b*-hexahydroindeno[1,2-*b*]indole-9,10-dione (4d). White solid (92% yield); m.p._{rep.} = 170–175 °C (ethanol); m.p._{lit.} = 160–162 °C;² IR (KBr) ν (cm⁻¹): 3465, 2957, 2883, 1722, 1602, 1489, 1148, 518; ¹H NMR (400 MHz, DMSO-*d*₆) δ (ppm) = 7.72 (t, *J* = 8.0 Hz, 3H, ArH), 7.61 (t, *J* = 8.0 Hz, 1H, ArH), 7.54 (t, *J* = 8.0 Hz, 1H), 7.35 (s, 1H), 7.26 (d, *J* = 8.0 Hz, 2H, ArH, OH), 6.68 (d, *J* = 8.0 Hz, 1H, ArH), 6.05 (s, 1H, OH), 2.42 (d, *J* = 16.0 Hz, 1H), 2.15 (d, *J* = 16.0 Hz, 1H), 1.90 (d, *J* = 16.0 Hz, 1H), 1.81 (d, *J* = 16.0 Hz, 1H), 0.95 (s, 3H, Me), 0.90 (s, 3H, Me).

2.7.5. 4*b*,9*b*-Dihydroxy-7,7-dimethyl-5-(naphthalene-1-yl)-4*b*,5,6,7,8,9*b*-hexahydroindeno[1,2-*b*]indole-9,10-dione (4e). Light yellow solid (93% yield); m.p._{rep.} = 200–205 °C (ethanol); m.p._{lit.} = 186–188 °C;³³ IR (KBr) ν (cm⁻¹): 3381, 2931, 1712, 1608, 1448, 1157; ¹H NMR (400 MHz, DMSO-*d*₆) δ (ppm) = 8.04–8.13 (m, 1H), 7.99 (d, *J* = 8.0 Hz, 1H, ArH), 7.93 (d, *J* = 8.0 Hz, 1H, ArH), 7.70–7.81 (m, 2H, ArH), 7.57–7.63 (m, 1H, ArH), 7.40–7.45 (m, 2H, ArH), 7.05–7.17 (m, 2H, ArH, OH), 6.36 (d, *J* = 8.0 Hz, 1H, ArH), 6.29 (d, *J* = 4.0 Hz, 1H, ArH), 6.02 (s, 1H, OH), 1.79–2.16 (m, 4H), 0.90 (s, 3H, Me), 0.78 (s, 3H, Me).

2.7.6. 5,5'-(1,4-Phenylene)bis(4*b*,9*b*-dihydroxy-7,7-dimethyl-4*b*,5,6,7,8,9*b*-hexahydroindeno[1,2-*b*]indole-9,10-dione) (4f). Smoky solid (95% yield); m.p._{rep.} = 305–310 °C (ethanol); IR (KBr) ν (cm⁻¹): 3357, 3176, 2960, 1719, 1567, 1507, 1449, 1380, 1157; ¹H NMR (400 MHz, DMSO-*d*₆) δ (ppm) = 7.77 (d, *J* = 8.0 Hz, 2H, ArH), 7.68–7.56 (m, 4H, ArH), 7.45–7.39 (m, 6H, ArH, OH), 6.75–6.79 (m, 2H, ArH), 6.09 (s, 2H, OH), 2.56 (d, *J* = 16.0 Hz, 2H), 2.18 (d, *J* = 16.0 Hz, 2H), 1.92 (d, *J* = 20.0 Hz, 4H), 1.02 (s, 6H, Me), 0.95 (s, 6H, Me); ¹³C NMR (100 MHz, DMSO-*d*₆) δ (ppm) = 198.06, 189.93, 163.66, 147.75, 136.13, 135.31, 130.93, 130.06, 129.81, 123.93, 106.68, 97.40, 83.91, 51.75, 37.56, 34.17, 34.13, 30.05.

2.7.7. 5-(2-Chlorophenyl)-4*b*,9*b*-dihydroxy-7,7-dimethyl-4*b*,5,6,7,8,9*b*-hexahydroindeno[1,2-*b*]indole-9,10-dione (4g). White solid (92% yield); m.p._{rep.} = 240–245 °C (ethanol); m.p._{lit.} = 230–231 °C;¹ IR (KBr) ν (cm⁻¹): 3417, 2955, 2874, 1714, 1571, 1446, 1155, 772; ¹H NMR (400 MHz, DMSO-*d*₆) δ (ppm) = 7.83 (d, *J* = 4.0 Hz, 1H, ArH), 7.74 (d, *J* = 8.0 Hz, 1H, ArH), 7.53–7.55 (m, 5H, ArH), 7.38 (s, 1H, OH), 6.66 (d, *J* = 4.0 Hz, ArH), 5.96 (s, 1H, OH), 2.08–1.95 (m, 4H), 0.97 (s, 3H, Me), 0.87 (s, 3H, Me).

2.7.8 4*b*,9*b*-Dihydroxy-5-(4-methoxyphenyl)-7,7-dimethyl-4*b*,5,6,7,8,9*b*-hexahydroindeno[1,2-*b*]indole-9,10-dione (4h). Gray solid (91% yield); m.p._{rep.} = 215–220 °C (ethanol); m.p._{lit.} = 224–226 °C;¹ IR (KBr) ν (cm⁻¹): 3410, 3037, 2951, 2715, 1728, 1607, 1512, 1441, 1149; ¹H NMR (400 MHz, DMSO) δ (ppm) = 7.72 (d, *J* = 8.0 Hz, 1H, ArH), 7.60–7.51 (m, 2H, ArH), 7.31–7.16 (m, 5H, ArH, OH), 6.66 (d, *J* = 8.0 Hz, 1H, ArH), 5.98 (s, 1H, OH), 2.39 (s, 3H, OMe), 2.35 (s, 1H), 2.13 (d, *J* = 16.0 Hz, 1H), 1.89 (d, *J* = 16.0 Hz, 1H), 1.77 (d, *J* = 16.0 Hz, 1H), 0.91 (s, 3H, Me), 0.88 (s, 3H, Me).

2.7.9. 5-(4-Chlorophenyl)-4*b*,9*b*-dihydroxy-7,7-dimethyl-4*b*,5,6,7,8,9*b*-hexahydroindeno[1,2-*b*]indole-9,10-dione (4i). White solid (93% yield); m.p._{rep.} = 223–228 °C (ethanol); m.p._{lit.} = 235–236 °C;¹ IR (KBr) ν (cm⁻¹): 3423, 2952, 1713, 1621, 1553, 1449, 1183, 771; ¹H NMR (400 MHz, DMSO-*d*₆) δ (ppm) = 7.73

(d, $J = 8.0$ Hz, 1H, ArH), 7.62–7.52 (m, 4H, ArH), 7.36 (s, 1H, OH), 7.33 (d, $J = 8.0$ Hz, 2H, ArH), 6.67 (d, $J = 8.0$ Hz, 1H, ArH), 6.06 (s, 1H, OH), 2.42 (d, $J = 20.0$ Hz, 1H), 2.15 (d, $J = 16.0$ Hz, 1H), 1.90 (d, $J = 16.0$ Hz, 1H), 1.80 (d, $J = 20.0$ Hz, 1H), 0.96 (s, 3H, Me), 0.90 (s, 3H, Me).

2.7.10. 5,5'-(Pyridine-2,6-diyl)bis(4*b*,9*b*-dihydroxy-7,7-dimethyl-4*b*,5,6,7,8,9*b*-hexahydroindeno[1,2-*b*]indole-9,10-dione) (4*j*). Pale yellow (94% yield); m.p._{rep.} = 215–220 °C (ethanol); IR (KBr) ν (cm⁻¹): 3389, 3254, 2943, 2879, 1713, 1660, 1607, 1464, 1255, 1164; ¹H NMR (400 MHz, DMSO-*d*₆) δ (ppm) = 8.34–8.21 (m, 2H, ArH), 8.87–7.43 (m, 11H, ArH, OH), 6.28 (s, 2H, OH), 2.37–1.99 (m, 8H), 1.03 (s, 6H, Me), 0.85 (s, 6H, Me); ¹³C NMR (100 MHz, DMSO-*d*₆) δ (ppm) = 197.55, 193.18, 175.94, 152.58, 147.25, 136.62, 134.70, 131.88, 125.30, 123.47, 112.94, 111.67, 91.09, 90.91, 82.60, 51.58, 37.63, 33.45, 27.81.

2.7.11. 5,5'-(Sulfonylbis(4,1-phenylene))bis(4*b*,9*b*-dihydroxy-7,7-dimethyl-4*b*,5,6,7,8,9*b*-hexahydroindeno[1,2-*b*]indole-9,10-dione) (4*k*). White solid (95% yield); m.p._{rep.} = 290–295 °C (ethanol); IR (KBr) ν (cm⁻¹): 3393, 2959, 2879, 1724, 1624, 1560, 1493, 1432, 1289; ¹H NMR (400 MHz, DMSO-*d*₆) δ (ppm) = 8.16–8.19 (m, 3H), 7.72 (d, $J = 4.0$ Hz, 2H), 7.65 (d, $J = 8.0$ Hz, 4H), 7.58 (s, 2H), 7.49–7.55 (m, 5H), 6.54–6.58 (m, 2H), 6.19 (s, 2H), 2.53–2.57 (m, 2H), 2.12–2.19 (m, 2H), 1.86–1.94 (m, 4H), 0.94 (s, 6H, Me), 0.88 (s, 6H, Me); ¹³C NMR (100 MHz, DMSO-*d*₆) δ (ppm) = 197.75, 190.35, 147.37, 142.04, 139.80, 135.51, 135.13, 130.89, 130.04, 129.03, 124.91, 123.85, 113.61, 108.00, 97.82, 83.98, 51.68, 37.55, 34.25, 29.86.

2.7.12. 4*b*,9*b*-Dihydroxy-7,7-dimethyl-5-(*o*-tolyl)-4*b*,5,6,7,8,9*b*-hexahydroindeno[1,2-*b*]indole-9,10-dione (4*l*). White solid (92% yield); m.p._{rep.} = 215–220 °C (ethanol); m.p._{lit.} = 217–216 °C; IR (KBr) ν (cm⁻¹): 3392, 2959, 1724, 1624, 1493, 1289, 1157; ¹H NMR (400 MHz, DMSO-*d*₆) δ (ppm) = 8.34 (s, 1H), 7.66–7.88 (m, 8H), 6.29 (s, 1H), 2.33 (s, 1H), 2.00–2.12 (m, 3H), 1.03 (s, 6H, Me), 0.85 (s, 3H, Me).

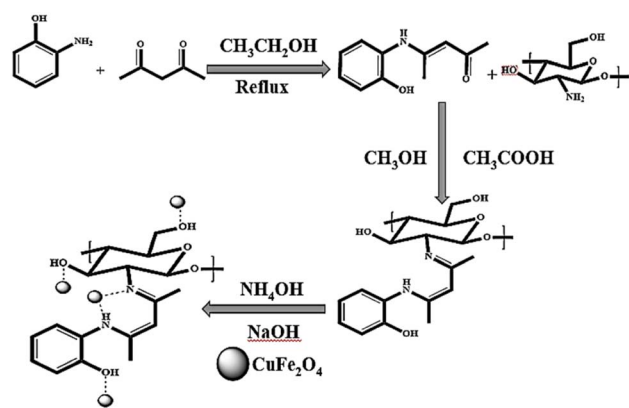
3. Results and discussion

3.1. Preparation and characterization of the CuFe₂O₄@CS-SB catalyst

The preparation of the CuFe₂O₄@CS-SB catalyst was done in three steps. In the first stage, the 4-(2-hydroxyaniline)pent-3-en-2-one Schiff base was prepared. The second stage is placing the desired Schiff base on the chitosan substrate and the third stage is chelating the copper ferrite nanoparticle with compounds on the chitosan and Schiff-base substrate. The general schematic of nanocatalyst preparation is shown in Scheme 1.

Furthermore, attenuated total reflectance (ATR), X-ray diffraction (XRD), field emission scanning electron microscopy (FE-SEM), elemental mapping, energy dispersive X-ray (EDX), thermogravimetric analysis (TGA), vibrational sample magnetometry (VSM) and Brunauer–Emmett–Teller (BET) analyses were used to characterize the CuFe₂O₄@CS-SB nanocomposite.

The ATR spectra of the Schiff base, Schiff base-chitosan and CuFe₂O₄@CS-SB catalyst are provided in the range from 400 to 4000 cm⁻¹ and are shown in Fig. 1. To detect the presence of the stretching vibration of the N–H and O–H bonds in the spectrum



Scheme 1 Preparation of the CuFe₂O₄@CS-SB catalyst.

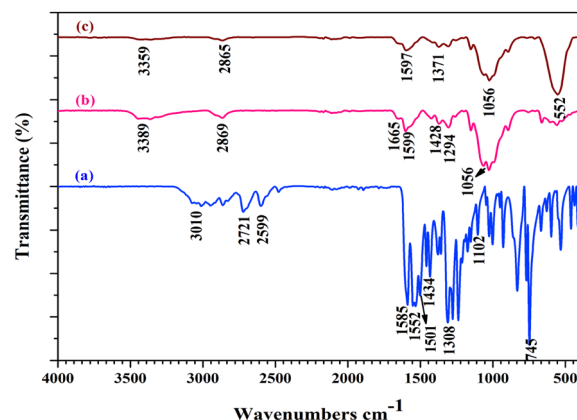


Fig. 1 ATR spectra of (a) Schiff base, (b) chitosan-Schiff base, (c) CuFe₂O₄@CS-SB catalyst.

of **1a**, a wide band was observed at the position of 3010 cm⁻¹. In the spectrum of **1a**, two absorption peaks in the region of 2721 and 2599 cm⁻¹ are related to the symmetric and asymmetric stretching vibrations of C–H (sp³), respectively. Due to the conjugated structure, the absorption peaks are 1585 cm⁻¹ and 1552 cm⁻¹ for the carbonyl and CH=NH groups, respectively. Two absorption peaks in the region of 1501 cm⁻¹ and 1434 cm⁻¹ are related to the stretching vibration of C=C in the aromatic ring, and the peak in the region of 745 cm⁻¹ is related to the alkene bond of =C–H (sp²). In the spectrum of **1b**, the stretching vibrations of O–H and N–H bonds have a broad peak at 3389 cm⁻¹ and C–H (sp³) as a weak peak at 2869 cm⁻¹. The peak observed at 1665 cm⁻¹ corresponding to the stretching vibrations of imine and the absorbed vibration of C=C of the aromatic ring appeared in the region of 1599 cm⁻¹ and 1428 cm⁻¹ and the stretching vibrations of the C–O–C appeared at 1056 cm⁻¹. In the spectrum of **1c**, the stretching vibrations of O–H and N–H bonds are in the region of 3359 cm⁻¹ and the stretching vibration of C–H (sp³) are in the region of 2865 cm⁻¹. The presence of stretching vibrations in the region of 1597 cm⁻¹ is due to the presence of the imine group and in at 1056 cm⁻¹ is related to C–O–C. The bonds related to metals such as Fe–O in

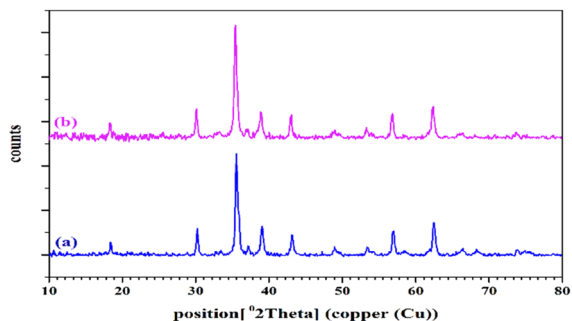


Fig. 2 X-ray diffraction spectra of (a) CuFe_2O_4 and (b) CuFe_2O_4 @CS-SB catalyst.

the 552 cm^{-1} region of self-vibration are visible in the ATR spectra.³⁴

The X-ray diffraction (XRD) patterns of (a) CuFe_2O_4 and (b) CuFe_2O_4 @CS-SB catalyst are shown in Fig. 2, which is a non-destructive technique to detect the crystal structure and state of phases. As can be seen in this figure, in the XRD pattern of CuFe_2O_4 , the crystal peaks for (220), (311), (222), (400), (422), (511) and (440) appeared, which is the reason for the presence of cubic CuFe_2O_4 with $Fd-3m$ space group (JCPDS No. card no 01-077-0010). The calculation of crystal formation using Scherrer's equation is reviewed in Table 1. The average particle size for this structure was measured to be 29.45 nm.

The field-emission scanning electron microscopy (SE-SEM) analysis for the CuFe_2O_4 @CS-SB catalyst was done and the related images are given in Fig. 3. The surface morphology and particle size of CuFe_2O_4 nanoparticles and CuFe_2O_4 @CS-SB nanocatalyst were investigated. These images show that the surface of the catalyst is rough, the nanoparticle shapes are mostly capsule-like and the average particle size range is 68.03 nm.

The elemental mapping analysis of the CuFe_2O_4 @CS-SB catalyst is shown in Fig. 4. With consideration of this figure, the images of elemental mapping show the distribution of C, N, O, Fe and Cu elements in this catalyst. As it is known, the active elements of catalysis are spread homogeneously on the catalyst substrate. The homogeneity of the elements on the catalyst substrate indicates that the entire surface of the catalyst has an active site that can show its catalytic effect by connecting this active site to the reaction.

Energy dispersive X-ray (EDX) analysis of the present catalyst is shown in Fig. 5. As seen in this pattern and the EDX specification table, there are carbon, oxygen, nitrogen, iron and copper in this catalyst and CuFe_2O_4 nanoparticles are uniformly dispersed on the chitosan-Schiff base (C K = wt%: 34.89 and

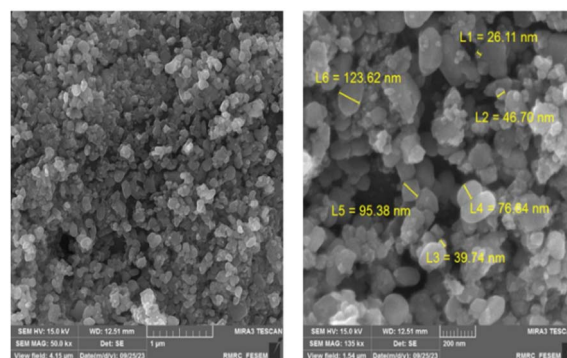


Fig. 3 FE-SEM images of the CuFe_2O_4 @CS-SB catalyst.

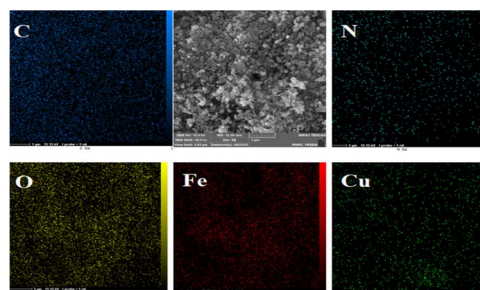


Fig. 4 Elemental mapping of the CuFe_2O_4 @CS-SB catalyst.

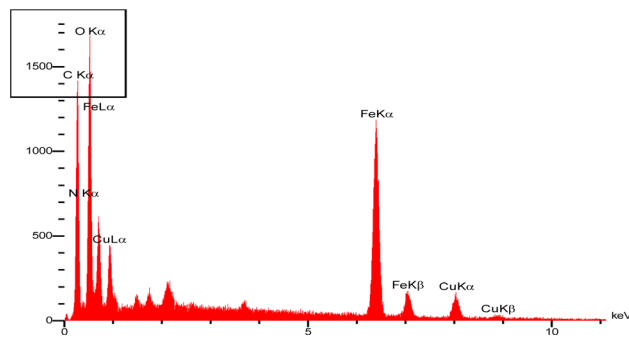


Fig. 5 The EDX of the CuFe_2O_4 @CS-SB catalyst.

at%: 51.48, N K = wt%: 5.82 and at%: 7.36, O K = wt%: 28.58 and at%: 31.66, Fe K = wt%: 24.36 and at%: 7.73, Cu K = wt%: 6.35 and at%: 1.77) (Table 2).

To investigate the thermal stability of chitosan and other organic materials, the thermogravimetric analysis (TGA) of the catalyst was done by increasing the temperature under nitrogen atmosphere (Fig. 6). As seen in this figure, the first weight loss at temperature below $200\text{ }^\circ\text{C}$, with a decrease of 1.58%, refers to the

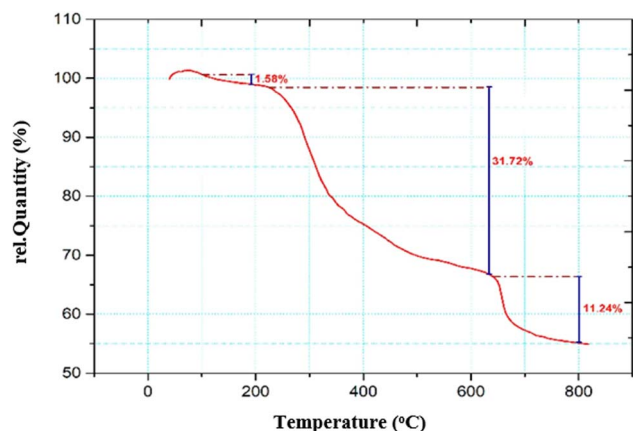
Table 1 The peak position, full width at half maximum ($\beta_{\frac{1}{2}}$), and calculated crystal size for nanoparticles^a

hkl	(220)	(311)	(222)	(400)	(422)	(511)	(440)
Peak position 2θ ($^\circ$)	30.0907	35.4090	38.9135	42.9803	53.3002	56.8027	62.3422
FWHM β ($^\circ$)	0.2362	0.2952	0.2952	0.2952	0.3542	0.3542	0.3542
Size (nm)	36.39	29.52	29.82	30.22	26.22	26.64	27.39

^a $\lambda = 0.154\text{ nm}$, $K = 0.94$.

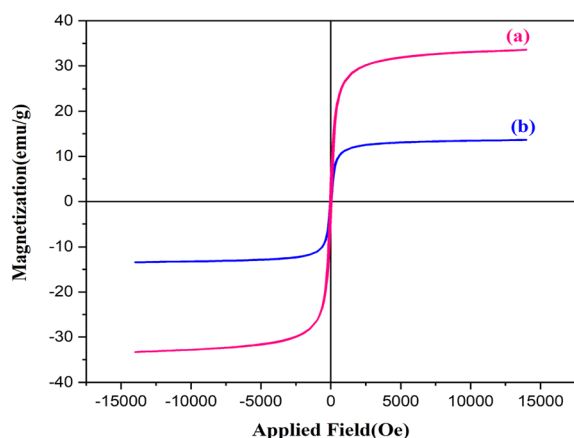
Table 2 EDX catalyst weight percent

Element	wt%	at%
C K	34.89	51.48
N K	5.82	7.36
O K	28.58	31.66
Fe K	24.36	7.73
Cu K	6.35	1.77

Fig. 6 TGA curve of the CuFe₂O₄@CS-SB catalyst.

removal of the absorbed water moisture. The second weight change from 245 to 600 °C, with the maximum peak of endothermic decomposition, proves the presence of organic groups and Schiff base attached to the chitosan. The third weight loss from 639 to 800 °C is related to the breaking of the chitosan polymer bonds.³⁵

Fig. 7 shows the vibrational sample magnetometry (VSM) curve of copper ferrite and the CuFe₂O₄@CS-SB catalyst. The saturation magnetism of the copper ferrite sample (a) is 33.50 emu g⁻¹ and that of the CuFe₂O₄@CS-SB catalyst sample (b) is 13.63 emu g⁻¹. It can be concluded that by introducing different

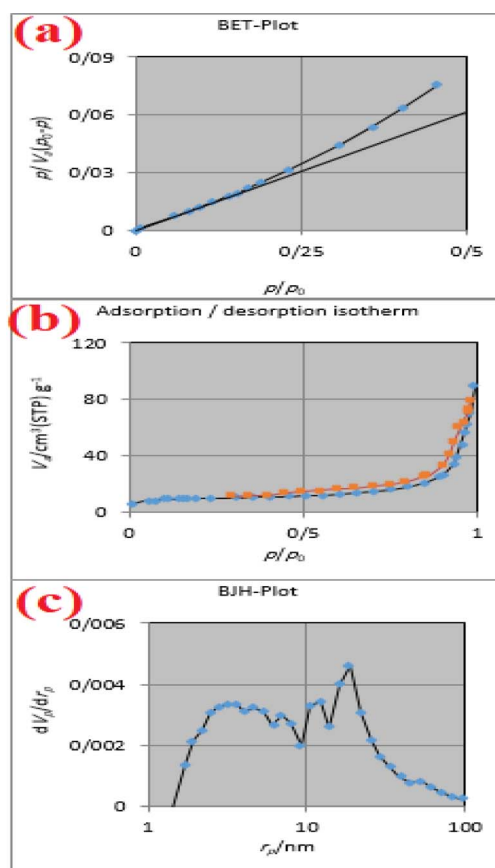
Fig. 7 The VSM curve of CuFe₂O₄ (a), CuFe₂O₄@CS-SB catalyst (b).

groups on the catalyst substrate, 19.87 emu g⁻¹ of the saturation magnetism of the nanocatalyst has been reduced, but the magnetism of the nanocatalyst is still maintained.

The Brunauer–Emmett–Teller (BET) in Fig. 8a for the CuFe₂O₄@CS-SB catalyst shows that the surface area was 35.34 m² g⁻¹, which increased the contact surface of the catalyst with the environment. The average pore diameter of the CuFe₂O₄@CS-SB catalyst is 15.06 nm and the total pore volume is 0.1331 cm³ g⁻¹, where the imine, hydroxyl, amino groups and copper ferrite nanoparticles have active adsorption, which is related to the type III adsorption–desorption isotherm (Fig. 8b). Also, the aggregates of the CuFe₂O₄@CS-SB catalyst are slit-like, according to this diagram (Fig. 8b). Based on the Barrett–Joyner–Halenda (BJH) method, Fig. 8c shows that the total pore volume (V_p) in the CuFe₂O₄@CS-SB catalyst is 0.1269 cm³ g⁻¹.

3.2. Catalytic activity evaluation of CuFe₂O₄@CS-SB

The multi-component cyclization reaction of aniline derivatives, dimedone and ninhydrin with a molar ratio of 1 : 1 : 1 using the CuFe₂O₄@CS-SB catalyst for the synthesis of indeno [1,2-*b*]indolones was carried out. First, the best reaction conditions were obtained from the optimization of the catalyst amount, solvent and temperature in the synthesis of these

Fig. 8 The BET curve (a), adsorption/desorption isotherm (b), the BJH curve (c) of the CuFe₂O₄@CS-SB catalyst.

organic compounds after comparison and detailed studies. Initially, different amounts of the catalyst in the reaction of dimedone (1 mmol), aniline (1 mmol) and ninhydrin (1 mmol) as a model reaction were investigated, and the best amount of the catalyst was reported to be 0.004 g (Table 3, entry 5).

Moreover, the model reaction was done in the presence of 0.004 g nanocatalyst at different temperatures, and the results are reported to Table 4. As indicated in this table, the best temperature at which excellent yield was obtained for this reaction was 75 °C (Table 4, entry 6).

Also, different polar and non-polar solvents were investigated to find out the best product yield and low reaction time, which gave the water as the solvent with excellent product yield formed in this reaction (Table 5, entry 9).

After optimization, in order to check the general applicability and develop the method, all kinds of aniline derivatives including electron donor and acceptor groups were used to prepare the indeno[1,2-*b*]indolone derivatives under the optimized conditions. The corresponding results are summarized in Scheme 2. As indicated in this scheme, the electron donating groups on the aniline ring are led to higher yields. As can be seen, short reaction times and excellent yields of the products are obtained due to the presence of the efficient catalyst. The physical and spectral data obtained from these compounds is the proof of the formation of these products.

Table 3 Optimization of the catalyst amount for the synthesis of 4a^a

Entry	Catalyst amount (g)	Time (min)	Yield ^b (%)
1	—	120	20
2	0.001	25	62
3	0.002	12	79
4	0.003	7	90
5	0.004	6	92
6	0.005	10	92

^a Reaction conditions: dimedone (1 mmol), aniline (1 mmol), ninhydrin (1 mmol) and CuFe₂O₄@CS-SB catalyst (0.004 g) at 75 °C. ^b Isolated yields.

Table 4 Optimization of temperature for the synthesis of 4a^a

Entry	Temperature (°C)	Time (min)	Yield ^b (%)
1	r.t	120	20
2	35	30	55
3	45	25	68
4	55	18	70
5	65	9	89
6	75	6	92
7	85	15	92

^a Reaction conditions: dimedone (1 mmol), aniline (1 mmol), ninhydrin (1 mmol) and CuFe₂O₄@CS-SB catalyst (0.004 g) in double distilled H₂O as the solvent at 75 °C. ^b Isolated yields.

Table 5 Optimization of solvent for the synthesis of 4a^a

Entry	Solvent	Time (min)	Yield ^b (%)
1	DMSO	19	73
2	DMF	43	60
3	EtOH	10	69
4	Acetone	60	28
5	THF	80	21
6	PEG	67	52
7	Toluene	100	17
8	CH ₃ CN	70	49
9	H ₂ O	6	92
10	H ₂ O/ethanol (1 : 1)	8	82

^a Reaction conditions: dimedone (1 mmol), aniline (1 mmol), ninhydrin (1 mmol) in the presence of CuFe₂O₄@CS-SB catalyst (0.004 g) in the selected solvent at 75 °C. ^b Isolated yields.

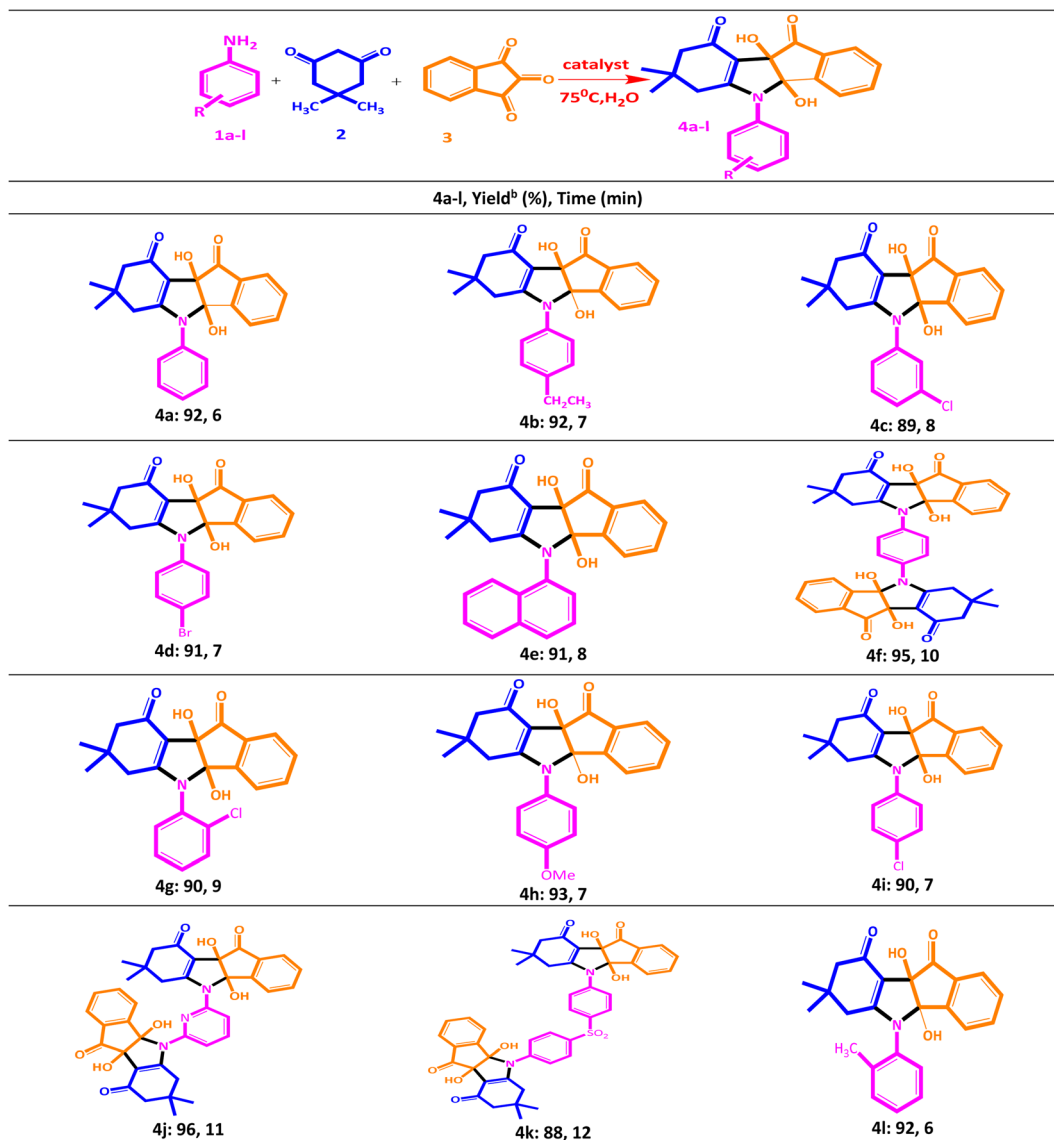
The results of the comparison of each of the four different products obtained using the current catalyst with four other previously reported catalysts for this reaction based on the product yield are shown in Table 6. It was concluded that with the CuFe₂O₄@CS-SB catalyst, shorter reaction time with excellent yield could be obtained under better thermal conditions.

3.3. Reusability of the catalyst

Since it is very important to recover the catalyst and reuse it, Fig. 9 shows the results of six runs of catalyst reuse. It has been concluded that during six runs of recycling, the yield decreased the least and the performance of the catalyst was excellent. To reuse the catalyst in subsequent reactions, the catalyst was separated using an external magnet, washed several times with ethanol and acetone, dried at 70 °C for 6 h and then can be reused. The short reaction times and excellent product yields are attributed to the efficiency of the catalyst. The physical and spectral data obtained from these compounds is the proof of the formation of these products.

In order to study the stability of the nanocatalyst, the FE-SEM image of the recovered catalyst was provided and is shown in Fig. 10. According to the image in Fig. 10a, the morphology of the catalyst did not change during reuse, indicating the structural resistance of the catalyst. Also, by examining the XRD pattern of the recovered catalyst, as shown in Fig. 10b, it is clear that after several steps of using the catalyst, it can be reused because the metals are still bound on the chitosan substrate.

In addition, the hot filtration method was used for the model reaction for the synthesis of 4a to investigate the leaching of the CuFe₂O₄@CS-SB catalyst. After 3 min of reaction time, the nanocatalyst was separated from the reaction mixture using a strong external magnet. The development of the reaction was monitored by thin layer chromatography (TLC), which concluded that no progress occurred in the reaction after the removal of the catalyst and so that leaching did not occur for the used catalyst.

Scheme 2 Synthesis of indeno[1,2-*b*]indolone derivatives^a.Table 6 Comparison of the catalytic activity of the CuFe₂O₄@CS-SB catalyst with other reported catalysts for the synthesis of indeno[1,2-*b*]indolone

Entry	Product	Conditions	Time (min)	Yield ^a (%)	Ref.
1	4i	MMT@Fe ₃ O ₄ (0.02 g, water, 70 °C)	7	90	This work
2			35	90	2
3	4d	SnO ₂ QDs (10 mol%, water, 70 °C)	7	91	This work
4			270	87	32
5	4a	Lactic acid (0.15 mmol, grind, 10 min, r.t)	6	92	This work
6			10	87	9
7	4b	C@TiO ₂ -SO ₃ H-ILs (0.1 g, water, 60 °C)	7	92	This work
8			60	92	1

^a Isolated yield.

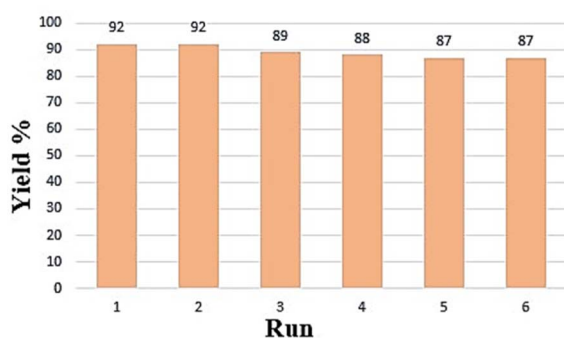


Fig. 9 The reusability of the $\text{CuFe}_2\text{O}_4@CS-SB$ catalyst.

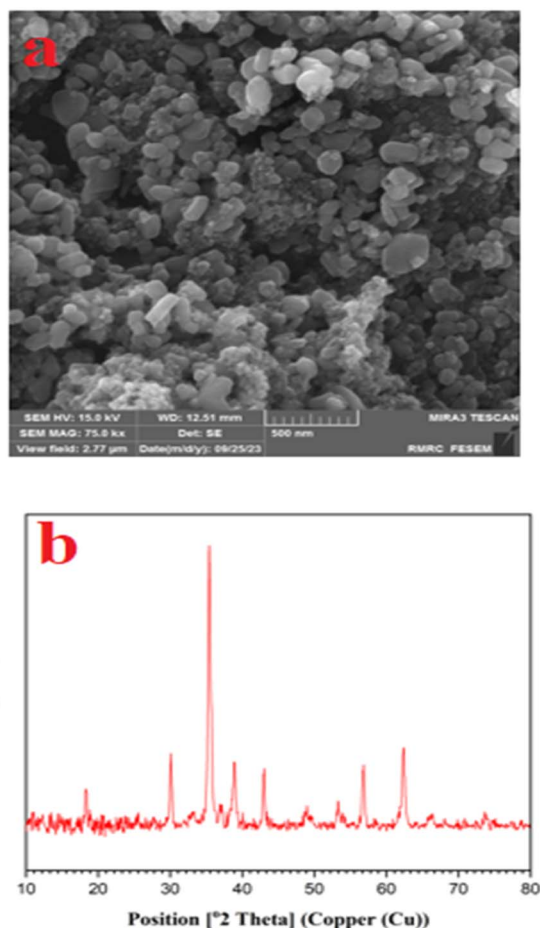


Fig. 10 FE-SEM (a) and XRD (b) images after reuse of the $\text{CuFe}_2\text{O}_4@CS-SB$ catalyst.

4. Conclusion

In this study, chitosan was prepared based on a Schiff base and chelated with copper ferrite. The FE-SEM, ^1H NMR, FT-IR, TGA, elemental mapping, EDX, BET and XRD analysis results confirmed that the $\text{CuFe}_2\text{O}_4@CS-SB$ catalyst was successfully synthesized. By comparing the FT-IR peaks of the catalyst in different stages of synthesis and also checking the ranges of

CuFe_2O_4 and Schiff base in XRD analysis, the formation of the catalyst was confirmed. As a result of these studies, the $\text{CuFe}_2\text{O}_4@CS-SB$ catalyst was employed for the synthesis of indeno[1,2-*b*]indolone derivatives under thermal conditions using water as the solvent.

Data availability

ESI† contains ^1H NMR, FT-IR and microscopy data.

Conflicts of interest

This paper's authors declare that they do not have any competing financial interests or personal relationships to influence their work.

Acknowledgements

The authors are grateful to the University of Kashan for supporting this work by Grant No. 159148/86.

References

- 1 M. Kour, M. Bhardwaj, H. Sharma, S. Paul and J. H. Clark, *New J. Chem.*, 2017, **41**, 5521–5532.
- 2 J. Safari and N. Hosseini Nasab, *Res. Chem. Intermed.*, 2019, **45**, 1025–1038.
- 3 R. R. Gupta, M. Kumar and V. Gupta, in *Heterocyclic Chemistry*, Springer Berlin Heidelberg, Berlin, Heidelberg, 1999, pp. 181–355.
- 4 A. W. Czarnik, *Anal. Chem.*, 1998, **70**, 378A–386A.
- 5 D. H. Kita, N. Guragossian, I. F. Zattoni, V. R. Moure, F. G. de M. Rego, S. Lusvarghi, T. Moulenat, B. Belhani, G. Picheth, S. Bouacida, Z. Bouaziz, C. Marminon, M. Berredjem, J. Jose, M. B. Gonçalves, S. V. Ambudkar, G. Valdameri and M. Le Borgne, *Sci. Rep.*, 2021, **11**, 1788.
- 6 X. Qian, R. Yan, C. Xu, L. Shao, H. Li and L. Hou, *J. Power Sources*, 2016, **332**, 103–110.
- 7 G. Lobo, M. Monasterios, J. Rodrigues, N. Gamboa, M. V. Capparelli, J. Martínez-Cuevas, M. Lein, K. Jung, C. Abramjuk and J. Charris, *Eur. J. Med. Chem.*, 2015, **96**, 281–295.
- 8 S. Haidar, Z. Bouaziz, C. Marminon, T. Laitinen, A. Poso, M. Le Borgne and J. Jose, *Pharmaceuticals*, 2017, **10**, 8.
- 9 X. Chen and Y. Liu, *Heterocycl. Commun.*, 2016, **22**, 161–163.
- 10 B.-C. Hong, Y.-F. Jiang, Y.-L. Chang and S.-J. Lee, *J. Chin. Chem. Soc.*, 2006, **53**, 647–662.
- 11 A. H. Ghasemi and H. Naeimi, *New J. Chem.*, 2020, **44**, 5056–5063.
- 12 L. C. Meher, C. P. Churamani, M. Arif, Z. Ahmed and S. N. Naik, *Renewable Sustainable Energy Rev.*, 2013, **26**, 397–407.
- 13 R. A. A. Muzzarelli, J. Boudrant, D. Meyer, N. Manno, M. DeMarchis and M. G. Paoletti, *Carbohydr. Polym.*, 2012, **87**, 995–1012.

- 14 A. H. Anwer, A. Ahtesham, M. Shoeb, F. Mashkoor, M. Z. Ansari, S. Zhu and C. Jeong, *Adv. Colloid Interface Sci.*, 2023, **318**, 102955.
- 15 H. Veisi, T. Tamoradi, A. Rashtiani, S. Hemmati and B. Karmakar, *J. Ind. Eng. Chem.*, 2020, **90**, 379–388.
- 16 J. Zhou, Z. Dong, H. Yang, Z. Shi, X. Zhou and R. Li, *Appl. Surf. Sci.*, 2013, **279**, 360–366.
- 17 M. N. V. Ravi Kumar, *Bull. Mater. Sci.*, 1999, **22**, 905–915.
- 18 F. Ali, S. B. Khan, T. Kamal, K. A. Alamry, E. M. Bakhsh, A. M. Asiri and T. R. A. Sobahi, *Carbohydr. Polym.*, 2018, **192**, 217–230.
- 19 F. G. Göze Özdemir, H. Çevik, J. C. Ndayiragije, T. Özek and İ. Karaca, *Int. J. Agric. Environ. Food. Sci.*, 2022, **6**, 410–416.
- 20 Q. Wei, Y. Wang, H. Wang, L. Qiao, Y. Jiang, G. Ma, W. Zhang and Z. Hu, *Carbohydr. Polym.*, 2022, **278**, 119000.
- 21 C. C. Berry, *J. Mater. Chem.*, 2005, **15**, 543–547.
- 22 Z. Guo, R. Xing, S. Liu, Z. Zhong, X. Ji, L. Wang and P. Li, *Carbohydr. Res.*, 2007, **342**, 1329–1332.
- 23 K. C. Gupta and A. K. Sutar, *Coord. Chem. Rev.*, 2008, **252**, 1420–1450.
- 24 P. Przybylski, A. Huczynski, K. Pyta, B. Brzezinski and F. Bartl, *Curr. Org. Chem.*, 2009, **13**, 124–148.
- 25 A. O. de Souza, F. C. S. Galetti, C. L. Silva, B. Bicalho, M. M. Parma, S. F. Fonseca, A. J. Marsaioli, A. C. L. B. Trindade, R. P. F. Gil, F. S. Bezerra, M. Andrade-Neto and M. C. F. de Oliveira, *Quim. Nova*, 2007, **30**, DOI: [10.1590/S0100-40422007000700012](https://doi.org/10.1590/S0100-40422007000700012).
- 26 R. Ghahremanzadeh, Z. Rashid, A. H. Zarnani and H. Naeimi, *Appl. Catal., A*, 2013, **467**, 270–278.
- 27 S. Kazempour and H. Naeimi, *Appl. Organomet. Chem.*, 2022, **36**, DOI: [10.1002/aoc.6903](https://doi.org/10.1002/aoc.6903).
- 28 S. Mousavi, H. Naeimi, A. H. Ghasemi and S. Kermanizadeh, *Sci. Rep.*, 2023, **13**, 10840.
- 29 A. Farazin, M. Mohammadimehr and H. Naeimi, *Int. J. Biol. Macromol.*, 2023, **241**, 124572.
- 30 S. Kermanizadeh, H. Naeimi and S. Mousavi, *Dalton Trans.*, 2023, **52**, 1257–1267.
- 31 A. H. Ghasemi, A. Farazin, M. Mohammadimehr and H. Naeimi, *Mater. Today Commun.*, 2022, **31**, 103513.
- 32 K. Pradhan, S. Paul and A. R. Das, *RSC Adv.*, 2015, **5**, 12062–12070.
- 33 M. U. Khan, R. A. Rather and Z. N. Siddiqui, *RSC Adv.*, 2020, **10**, 44892–44902.
- 34 A. Massoud-Sharifi, G. K. Kara and M. Rabbani, in *The 4th International Electronic Conference on Water Sciences*, MDPI, Basel Switzerland, 2019, p. , p. 17.
- 35 R. Antony, S. Theodore David, K. Saravanan, K. Karuppasamy and S. Balakumar, *Spectrochim. Acta, Part A*, 2013, **103**, 423–430.